Chemical Preintercalation Synthesis Approach for the Formation of New Layered Tungsten Oxides

Mallory Clites[a], Adam Blickley[a], David A. Cullen[b], Ekaterina Pomerantseva[a]*

[a] Department of Materials Science and Engineering, Drexel University, Philadelphia, PA 19104, USA

[b] Center for Nanophase Materials Sciences, Oak Ridge National Laboratory, Oak Ridge, TN 37831, USA

* Corresponding author: ep423@drexel.edu

Keywords: chemical preintercalation; tungsten oxide; layered materials; confined water; energy storage

ABSTRACT

Tungsten oxide, $WO_3 \cdot nH_2O$, is a unique layered oxide material that offers enhanced performance in electrochromic and energy storage applications. Herein, we report the formation of a new, never previously synthesized, Na-containing layered tungsten oxide phase, $Na_{0.20}WO_3 \cdot 0.81H_2O$, using a chemical preintercalation approach. The structure and composition of this novel phase were investigated via microscopy, spectroscopy, and diffraction methods. Electrochemical cycling of $Na_{0.20}WO_3 \cdot 0.81H_2O$ electrodes revealed initial discharge capacities of 37.43 mAh g^{-1}, 480.8 mAh g^{-1}, and 253.2 mAh g^{-1} in aqueous H_2SO_4 cells (potential window of -0.2– 0.8 V vs. Ag/AgCl), non-aqueous Li-ion cells (potential window of 0.1 – 4.0 V vs. Li/Li^+), and non-aqueous Na-ion cells (potential window of 0.1 – 4.0 V vs. Na/Na^+), respectively. Additionally, a reversible, pressure-induced color change from pale yellow to dark brown/black was observed for the $Na_{0.20}WO_3 \cdot 0.81H_2O$ sample when it was placed under pressures of 1000 psi or higher. Our results demonstrate the viability of chemical preintercalation synthesis approach to produce new oxide phases with interesting functional properties.

GRAPHICAL ABSTRACT

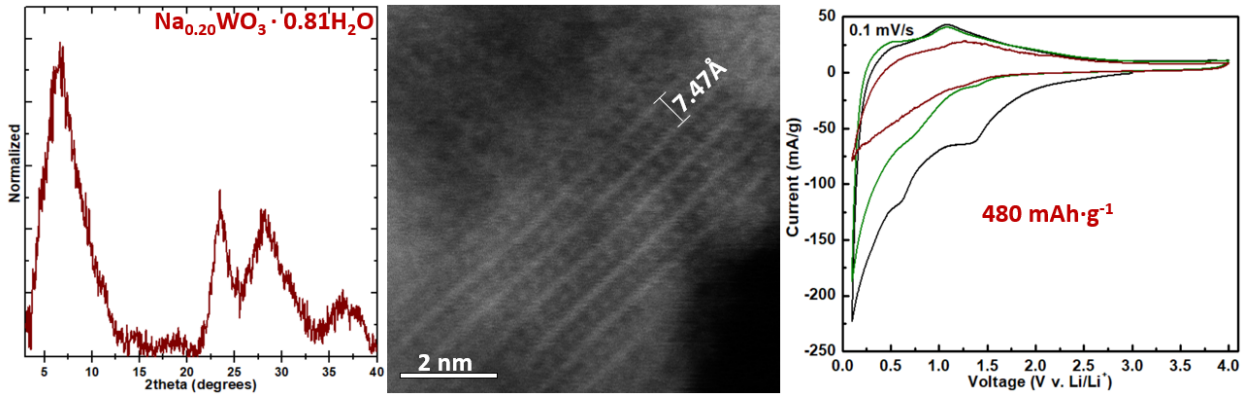

INTRODUCTION

The discovery and synthesis of new materials can lead to breakthroughs in technology development, while the opportunities to create new materials rely on chemical processes enabling control over atoms positioning at the desired locations in a crystal structure. Specifically, the synthesis of new layered transition metal oxides is highly pursued due to their advantages in electrochemical applications, such as energy storage and electrochromics. Among these phases, tungsten oxides are of particular interest because of their excellent electrochromic properties, semiconductor behavior, pseudocapacitive energy storage mechanism, and facile synthesis [1-6]. It was shown that the presence of interlayer water in the structure of layered tungsten oxides enables high-rate electrochemical proton intercalation and promotes stability by minimizing electrochemically driven deformation [7-9]. $WO_3 \cdot nH_2O$ has a layered structure built from corner-sharing WO_6 octahedra which crystallize into monoclinic, triclinic, tetragonal, orthorhombic, and cubic phases depending on synthesis and processing parameters [10, 11]. The most widely studied polymorphs of the hydrated tungsten oxides are $WO_3 \cdot H_2O$ and $WO_3 \cdot 2H_2O$. Schematic illustrations of their crystal structures are shown in **Figure S1** of the **Supporting Information**. The interlayer spacing in $WO_3 \cdot nH_2O$ can vary from 4 to 7 Å, depending on the degree of hydration, *n,* which typically falls between 0.33 and 2.0 [6, 12]. While interest in $WO_3 \cdot nH_2O$ polymorphs was initially sparked by their electrochromic properties, hydrated tungsten oxides recently emerged as promising electrode materials for energy storage systems, including aqueous pseudocapacitors [8, 13] and non-aqueous Li-ion [14-16] and Na-ion cells [17, 18]. In non-aqueous cells, the electrochemical stability of this phase remains a challenge due to the poorly reversible conversion reaction which takes place between tungsten oxide and Li^+/Na^+ ions [6, 16]. New layered tungsten oxides, stabilized by interlayer water molecules, can be an interesting alternative to investigate charge storage properties and shed light on the electrochemistry of this class of materials.

The chemical preintercalation synthesis approach consists of a modified low-temperature sol-gel or precipitation process, and it allows for the fabrication of layered transition metal oxides with large interlayer region stabilized by inorganic cations and interlayer water molecules [19-24]. Chemical preintercalation of organic molecules has also been reported [25, 26]. The ability to utilize a large library of chemically preintercalated species opens opportunities to synthesize a versatile family of novel materials with advanced functionalities and previously unknown properties. For example, it was shown that chemical preintercalation of ions or molecules into the

materials crystal structure suppressed electrochemically induced lattice reconstruction leading to enhanced stability [21, 27]. In energy storage, it was established that rationally designed chemical preintercalation can also lead to improved ion diffusion and electronic conductivity [23]. Chemically preintercalated vanadium [19-21], titanium [28] and molybdenum [22, 24] oxides have been reported. However, up until now this synthesis approach remained unexplored in the case of tungsten oxides.

Herein, we report the first realization of the chemical preintercalation method for the synthesis of a new Na-preintercalated layered hydrated tungsten oxide phase, $Na_{0.20}WO_3 \cdot 0.81H_2O$. The chemical composition was determined using EDX spectroscopy and TGA weight loss curves. The details of the material structure were obtained through XRD, Raman spectroscopy and FTIR spectroscopy characterization. STEM imaging revealed that while this novel $Na_{0.20}WO_3 \cdot 0.81H_2O$ material has a layered structure, it does not resemble any of the previously reported tungsten oxide phase. The novel atomic arrangement could be attributed to the low temperature used in a precipitation reaction-based synthesis route and presence of the chemically preintercalated ions in the reaction mixture inducing specific interactions that lead to new crystallization pathways. The initial charge storage properties of the $Na_{0.2}WO_3 \cdot 0.81H_2O$ phase were evaluated in electrochemical cells with aqueous and non-aqueous electrolytes. In addition, a reversible, pressure-induced color change of the $Na_{0.2}WO_3 \cdot 0.81H_2O$ sample was found. This study aims to better understand the novel sodium-tungsten oxide material as well as highlight the versatility of the chemical preintercalation approach to synthesize a variety of layered transition metal oxide phases.

EXPERIMENTAL METHODS

Synthesis

Synthesis of Pristine $WO_3 \cdot H_2O$

Pristine $WO_3 \cdot H_2O$ samples were synthesized following methods previously reported elsewhere [1, 4, 10]. Briefly, 1.12g of tungsten powder (Fisher Scientific, USA) was added to a beaker containing 50 mL of $H_2O_{2(aq)}$ (30 wt%, Fisher Scientific, USA) over the course of 5 minutes. An ice bath was used to prevent a run-away exothermic reaction between the peroxide and the tungsten powder. After all metal powder was added, the ice bath was removed. The dark-grey suspension was stirred

vigorously at 40°C for ~1 hour until all metal dissolved indicated by the formation of a transparent, clear solution. The temperature was next raised to 80°C. After 2 hours, the solution color changed to an opaque light yellow. The beaker was then covered with aluminum foil and the solution was kept at 100 °C for ~18 hours until all liquid evaporated. A bright yellow powder was the final product.

Synthesis of Chemically Preintercalated $Na_xWO_3 \cdot nH_2O$

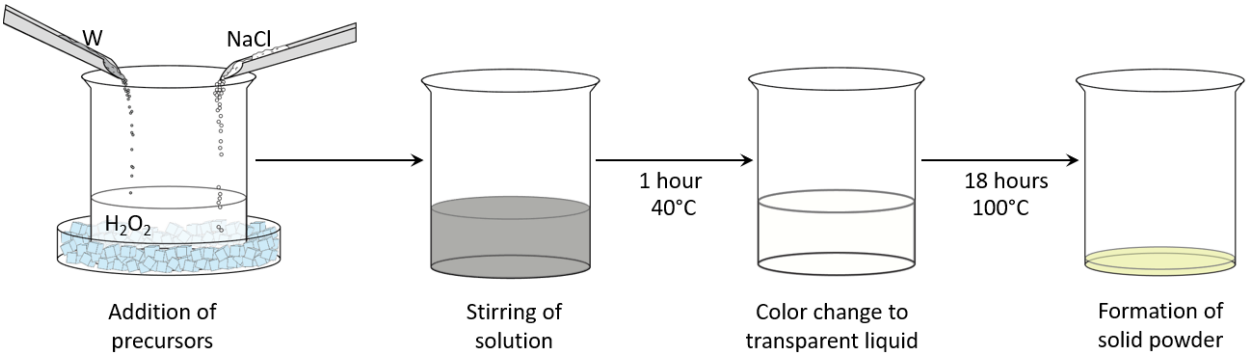

Figure 1. Schematic representation of the chemical pre-intercalation approach used to synthesize $Na_xWO_3 \cdot nH_2O$ samples.

Chemically preintercalated $Na_xWO_3 \cdot nH_2O$ samples were synthesized by adapting the above-described procedure for the preparation of pristine $WO_3 \cdot nH_2O$ as well as the chemical pre-intercalation approach developed for layered vanadates and titanates [19-21, 28]. In this process, 50 mL of $H_2O_{2(aq)}$ (30 wt%, Fisher Scientific, USA) was added into a beaker on ice. Metallic tungsten and NaCl powders (Fisher Scientific, USA) were added to the solution with a precursor ratio of Na:W 5:1 over the course of 5 minutes. After all precursor powders were added, the ice bath was removed. The synthesis process then followed the same steps as those described above. The final product was a pale-yellow fine powder.

Materials Characterization

The morphology and chemical composition of the synthesized materials were studied using scanning electron microscopy (SEM, Zeiss Supra 50VP, Germany) equipped with an energy dispersive X-ray (EDX) spectroscopy attachment. EDX was used to determine the Na:W ratio in the synthesized samples. EDX spectra were obtained in 10 µm × 10 µm areas of each sample and

the Na:W was calculated by averaging the data from the three spectra taken from different sample regions. Thermal stability and structural water content were evaluated using thermogravimetric analysis (TGA, Q50, TA Instruments, USA). The temperature induced weight loss was evaluated by heating the samples from room temperature to 1000°C with a heating rate of 10 °C min^{-1} in air. X-ray diffraction (XRD) patterns were collected with a Rigaku Miniflex diffractometer (Japan) with Cu Kα radiation. High-angle annular dark-field (HAADF) and bright-field (BF) aberration-corrected scanning transmission electron microscopy (STEM) images were acquired at an accelerating voltage of 300 keV with a FEI Titan microscope equipped with Schottky source and CEOS probe corrector. Further structural information was gathered using Fourier transform infrared (FTIR) spectroscopy and Raman spectroscopy. FTIR spectra were recorded using a Perkin-Elmer spectrometer between 500 and 3600 cm^{-1}, and Raman spectra were collected from 200 to 1100 cm^{-1} using a Renishaw inVia spectrometer with a red 633 nm light source.

Electrochemical Testing

Electrochemical testing in non-aqueous electrolytes was carried out using 2032 type two electrode coin cells with Li or Na metal (Sigma Aldrich) serving as the counter and reference electrodes. The working electrode was composed of 70 wt. % active material, 20 wt. % acetylene black, and 10 wt. % polyvinyl difluoride (PVDF, Arkema, USA) binder. The constituents were dispersed in N-methylpyrrolidone (NMP, Fisher Scientific, USA) and the produced slurry mixture was cast onto an Al foil via doctor blade. Disks (12 mm diameter) were punched from the film and dried at 100 ^{o}C for 12 hours under vacuum. For Li-ion cells, a solution composed of 1 M $LiPF_6$ in 1:1 ethylene carbonate: diethylene carbonate (EC:DEC) (LP40, BASF, USA) was used as electrolyte. Celgard was used as the separator (Celgard, USA). For Na-ion cells, an electrolyte solution was composed of 1 M $NaClO_4$ (Sigma Aldrich, USA) in 1:1 ethylene carbonate : propylene carbonate (EC:PC) with 5 wt. % fluoroethylene carbonate (FEC) additive (BASF, USA). Glass microfiber was used as the separator (Whatman, USA).

Electrodes in the cells with an aqueous electrolytes consisted of 80 wt. % active material, 10 wt. % carbon black and 10 wt. % polytetrafluoroethylene (PTFE) binder. The electrodes were produced by dispersing the three components in ethanol and stirring overnight as the ethanol evaporated to ensure a homogeneous mixture. The mixture was then repeatedly rolled and pressed,

with ethanol being added periodically to allow for a malleable consistency until a film was produced. Counter electrodes were prepared through the same process but with a ratio of 91.5 wt. % YP50 and 8.5 wt. % PTFE. The counter electrodes were punched into 12mm discs that weighed at least 10x that of the working electrodes to ensure that the limiting part of the electrochemical device was the active material-containing working electrode. The mass of the working electrodes was ~0.3 mg. Electrochemical testing was carried out in three-electrode Swagelok cells with platinum discs serving as current collectors, Celgard film as the separator, and Ag/AgCl as reference electrodes. 1M H_2SO_4, 1 M Na_2SO_4, and 1 M NaOH solutions were used as electrolytes.

Cyclic voltammetry data were collected on a BioLogic VMP-3 multichannel workstation (Biologic, France) at a scan rate of 0.1 mV/s. Electrochemical testing was carried out in the potential window of 0.1-4.0 V vs Li/Li^+ or Na/Na^+ for non-aqueous cells. In aqueous cells, cycling was carried out in the potential window of -0.2 – 0.8 V vs Ag/AgCl with 1M H_2SO_4 electrolyte, -0.7 – 0.3 V vs Ag/AgCl with 1M NaOH electrolyte, and -0.4 – 0.6 V vs Ag/AgCl with 1M Na_2SO_4 electrolyte. All potentials in aqueous cells are reported vs the Ag/AgCl reference electrode, while the potentials in non-aqueous Li-ion and Na-ion cells are reported vs Li/Li^+ and Na/Na^+ reference electrodes, respectively.

For an individual cycle at a particular scan rate, specific capacitance (F/g) was determined from the absolute integral area within the CV curve, the active mass of the electrode (m), the potential sweep rate (v), and the potential window (ΔV) according to Equation 1.

$$Specific\ capacitance = \frac{\int I\, dV}{2mv\Delta V} \qquad (Equation\ 1)$$

Pressure Testing

$Na_{0.20}WO_3 \cdot 0.81H_2O$ pellets were pressed at room temperature using an 11 mm (0.433 inch) die punch (Across International, USA) at increasing pressures from 1000 to 5000 psi and ~1-2 mins holding time in a Carver hydraulic press (Carver, USA).

RESULTS AND DISCUSSION

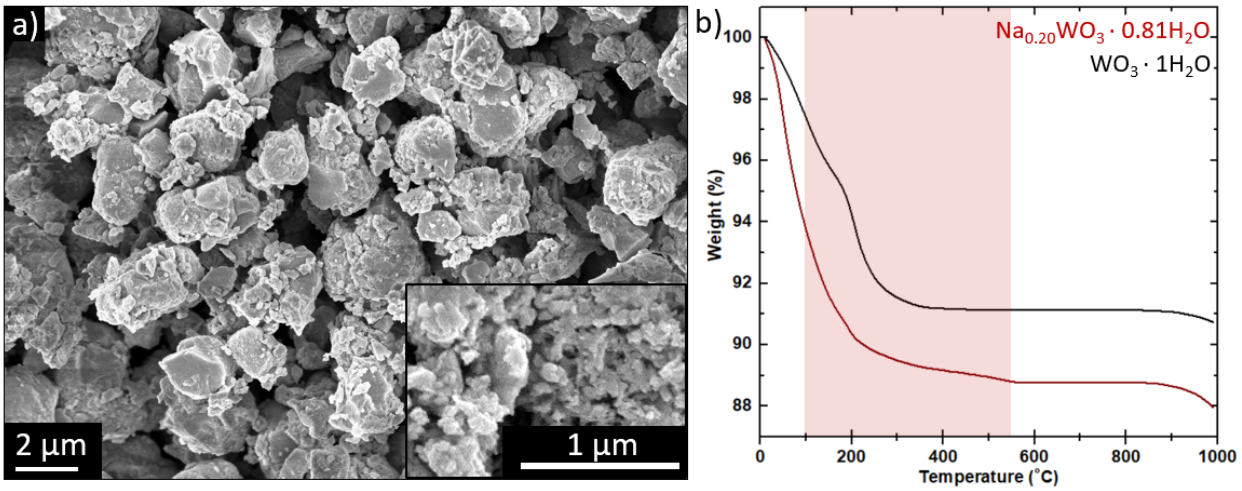

Figure 2. (a) SEM image of a $Na_xWO_3 \cdot nH_2O$ sample; the inset shows a region with higher magnification. (b) TGA data for $WO_3 \cdot nH_2O$ and $Na_xWO_3 \cdot nH_2O$ samples. The temperature region highlighted with light red rectangle was used to evaluate the hydration degrees.

Figure 2a shows the SEM image of the $Na_xWO_3 \cdot nH_2O$ material. The morphology of the material appears as spherical particles, some of which are built from nanoflakes. While some bulk particles are observed, many small particles ~100 nanometers in diameter are also visible. The inset in **Figure 2a** shows an image at higher magnification where the small nanoparticles can be more easily identified. EDX spectra were obtained for the $WO_3 \cdot nH_2O$ and $Na_xWO_3 \cdot nH_2O$ samples (**Supporting Information, Figure S2**). Pre-intercalation of Na^+ ions into the structure of the $Na_xWO_3 \cdot nH_2O$ sample was confirmed by the presence of Na peaks in the spectra that were not observed for the pristine $WO_3 \cdot nH_2O$ sample. A Na:W ratio of 0.2 was determined, which corresponds to an empirical formula of $Na_{0.20}WO_3 \cdot nH_2O$. Based on the lack of Cl peaks in the EDX spectra for the $Na_{0.20}WO_3 \cdot nH_2O$ sample, we conclude that all Na^+ ions are present in the structure of the synthesized complex tungsten oxide and no NaCl impurity remained in the material after washing.

Figure 2b shows the TGA data obtained for the $WO_3 \cdot nH_2O$ and $Na_{0.20}WO_3 \cdot nH_2O$ samples. Below 100°C, weight loss in both samples is attributed to the loss of physisorbed water. For the pristine $WO_3 \cdot nH_2O$ sample, a weight loss of 7.25% between 100-550°C was ascribed to the loss of crystallographically-bound water molecules within the structure. This weight loss corresponds to

an n of 1.0 in $WO_3 \cdot nH_2O$, which is the expected water content in this sample based on previous synthesis studies. In the same temperature range, $Na_xWO_3 \cdot nH_2O$ material demonstrated a weight loss of 5.87%, which corresponds to a value of n of 0.81. The lower water content in the preintercalated $Na_{0.20}WO_3 \cdot 0.81H_2O$ material as compared to the pristine $WO_3 \cdot 1H_2O$ sample may be due to the intercalation of Na^+ ions that resulted in fewer intercalated water molecules. Alternatively, this result could be due to the formation of a different phase when Na^+ ions are incorporated into the structure.

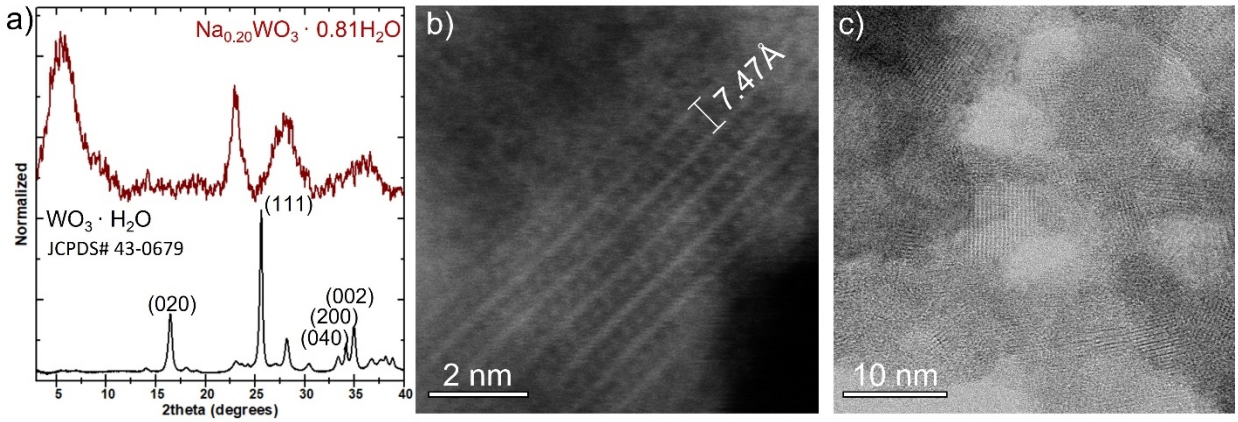

Figure 3. (a) XRD patterns of $WO_3 \cdot 1H_2O$ and $Na_xWO_3 \cdot 0.81H_2O$ samples. (b) HAADF and (c) BF-STEM images of the $Na_{0.20}WO_3 \cdot 0.81H_2O$ sample.

Figure 3a shows the XRD patterns of the pristine $WO_3 \cdot 1H_2O$ and preintercalated $Na_{0.20}WO_3 \cdot 0.81H_2O$ samples. The XRD pattern of $WO_3 \cdot nH_2O$ exhibits two high intensity peaks at ~16° and 26° 2θ and several smaller peaks at 18°, 23°, 28°, 30°, 33°, 34°, 35°, 37°, 38°, and 39° 2θ, that were indexed to the $WO_3 \cdot 1H_2O$ phase (JCPDS# 43-0679) [29]. However, the XRD pattern of the chemically preintercalated $Na_{0.20}WO_3 \cdot 0.81H_2O$ sample could not be indexed to any pattern of the previously synthesized Na- and W-containing oxides. The closest XRD pattern found in literature is the one for a layered WO_3 phase containing interlayer Mn^{2+} ions [30]. An XRD pattern with peaks of decreasing intensities at 5.64°, 22.5°, 28° and 37° 2θ resembles patterns observed for layered oxide phases with large interlayer spacings [19, 21, 31]. If the peak occurring at 5.64° 2θ in the XRD pattern corresponded to the d-spacing of this material, the calculated interlayer spacing from this peak would be 15.66 Å. However, given the lack of similar XRD patterns in literature, and the overall low intensity of this pattern, which may be attributed to low crystallinity or a high-degree of nano-structuring in this sample, indexing of this pattern is not possible. Low

crystallinity of open-layered structures has been discussed previously for other transition metal oxides synthesized via sol-gel or precipitation reaction routes [32, 33]. The low crystallinity makes it difficult to use typical indexing or Rietveld refinement techniques. More in-depth pair distribution function (PDF) refinement would be required [33]. Determining the structure of the synthesized material is necessary to understand the discrepancy between the XRD and STEM data.

As such, STEM imaging was used to further understand the structure of the synthesized $Na_{0.20}WO_3 \cdot 0.81H_2O$ material (**Fig. 3b and 3c**). The HAADF-STEM image in **Figure 3b** shows that the $Na_{0.20}WO_3 \cdot 0.81H_2O$ nanoflakes are built from layers separated by an interlayer spacing of ~7.47 Å. This interlayer spacing is approximately half that anticipated from the XRD pattern of the phase, suggesting that the peak at 5.64° 2θ in the XRD pattern corresponds to a reflection found in alternating W-O layers. Therefore, the true interlayer spacing between two W-O layers is a half of that value. The W-O layers appear to be built from distorted polyhedra, as individual polyhedra cannot be resolved, but rather bright bands are visible. This is in agreement with the distortions seen in WO_3 layers which result in a phase change from a highly ordered cubic structure to a distorted triclinic structure [11]. Within the interlayer space, bright, individual dots can be recognized. These dots may be columns of atoms or small polyhedra. Given the intensity of the columns, and the relatively low Na:W ratio obtained from EDX spectroscopy measurements, it is unlikely that these are Na^+ ions residing in the structure. The lack of any other elements appearing in the EDX spectra suggests that these atoms may in fact be tungsten atoms or WO_x polyhedra residing between the W-O layers. **Figure 3c** shows several thin and overlapping nanoflakes, all with the same layered structure and interlayer atoms observed in **Figure 3b.** To the best of our knowledge, no other previously studied Na- and W-containing oxides show this same layered structure. Pristine $WO_3 \cdot 1H_2O$ typically shows an interlayer spacing of ~4.3 Å, significantly smaller than the 7.47 Å observed in the Na-preintercalated tungsten oxide structure. Park et al. previously synthesized a hexagonal, layered $Na_{0.17}WO_{3.085} \cdot 0.17H_2O$ structure for use in electrocatalysis [31]. While this structure contains a similar Na:W ratio as our synthesized $Na_{0.20}WO_3 \cdot 0.81H_2O$ material, the interlayer spacing is considerably smaller (3.89 Å compared to 7.47 Å). Rather, the layered $Na_{0.17}WO_{3.085} \cdot 0.17H_2O$ structure more closely matches the structure of the pristine, $WO_3 \cdot 1H_2O$ phase [31].

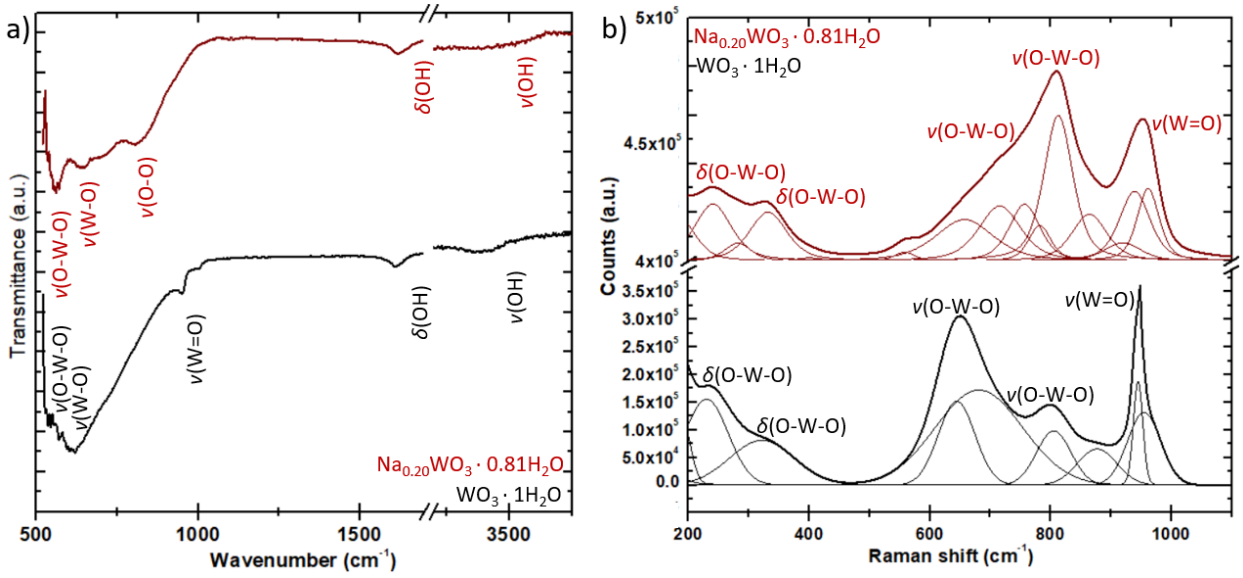

Figure 4. (a) FTIR and (b) Raman spectra of $WO_3 \cdot 1H_2O$ and $Na_{0.20}WO_3 \cdot 0.81H_2O$ samples.

Figure 4 shows the FTIR and Raman spectra of the pellets pressed from $WO_3 \cdot 1H_2O$ and $Na_{0.20}WO_3 \cdot 0.81H_2O$ samples. FTIR modes are shown in **Table 1**. The Raman spectra band analysis for both samples is presented in **Table 2**. O-H stretching (3200-3600 cm^{-1}) and bending (~1620 cm^{-1}) bands are clearly visible in the FTIR spectra, confirming the TGA data that shows the presence of crystallographic water in both samples. A sharp W=O band at 952 cm^{-1} is observed for the $WO_3 \cdot 1H_2O$ sample that is not visible for the preintercalated $Na_{0.20}WO_3 \cdot 0.81H_2O$ sample [34, 35]. Instead, a broader O-O stretching band appears in the FTIR spectrum of this phase at 796 cm^{-1}. Further, the ν(O-W-O) and ν(W-O) bands at 559 and 636 cm^{-1} are significantly sharper than those found in the FTIR spectrum of the $WO_3 \cdot 1H_2O$ sample at 560 and 620 cm^{-1}. The differences between these band intensities suggest that the W=O bond in the preintercalated $Na_{0.20}WO_3 \cdot 0.81H_2O$ sample becomes significantly weaker while the W-O and O-W-O bonding increases. This explanation is further confirmed via Raman spectroscopy, where the sharp W=O band found at 950 cm^{-1} for the $WO_3 \cdot 1H_2O$ sample becomes less intense and broader upon sodium preintercalation. In addition, the ν(O-W-O) stretching band in the pristine sample shows distinct splitting in the peaks, with two peaks found at 644 & 680 cm^{-1} and at 804 & 876 cm^{-1}. In contrast, the Raman spectrum of Na-preintercalated sample displays seven highly overlapping peaks [34, 36, 37]. Overall, the O-W-O bond in the $Na_{0.20}WO_3 \cdot 0.81H_2O$ sample shifts to higher cm^{-1}, which suggests that this bond becomes stronger. The peak fitting in the Raman spectrum of the new $Na_{0.20}WO_3 \cdot 0.81H_2O$ material is based on literature data describing Raman bands in tungsten

oxides; however, the true interpretation of the Raman spectrum, including the physical meaning of each spectrum feature, requires knowledge of the material structure which is currently unavailable. The FTIR and Raman spectroscopy data suggests that while there are certain similarities in the bonding of the reference $WO_3 \cdot 1H_2O$ and new $Na_{0.20}WO_3 \cdot 0.81H_2O$ materials, these two phases are not identical. These results are in agreement with the XRD and TEM characterization that revealed the unique structure of the $Na_{0.20}WO_3 \cdot 0.81H_2O$ phase which is different from the structure of the reference $WO_3 \cdot 1H_2O$ material.

Table 1. FTIR peak modes for $WO_3 \cdot 1H_2O$ and $Na_{0.20}WO_3 \cdot 0.81H_2O$ samples.

$WO_3 \cdot 1H_2O$		**$Na_{0.20}WO_3 \cdot 0.81H_2O$**	
546	ν(O-W-O)	559	ν(O-W-O)
560			
		636	ν(W-O)
620	ν(W-O)	696	
952	ν(W=O)	799	ν(O-O)
1618	δ(O-H)	1623	δ(O-H)
3392	ν(O-H)	3399	ν(O-H)

Table 2. Raman fitted bands for $WO_3 \cdot 1H_2O$ and $Na_{0.20}WO_3 \cdot 0.81H_2O$ samples.

$WO_3 \cdot 1H_2O$		**$Na_{0.20}WO_3 \cdot 0.81H_2O$**	
231	δ(O-W-O)	242	
325		285	δ(O-W-O)
		332	
644			
680	ν(O-W-O)	556	
804		658	
876		712	
		756	ν(O-W-O)
945	ν(W=O)	779	
953		814	
		865	
		921	
		937	ν(W=O)
		961	

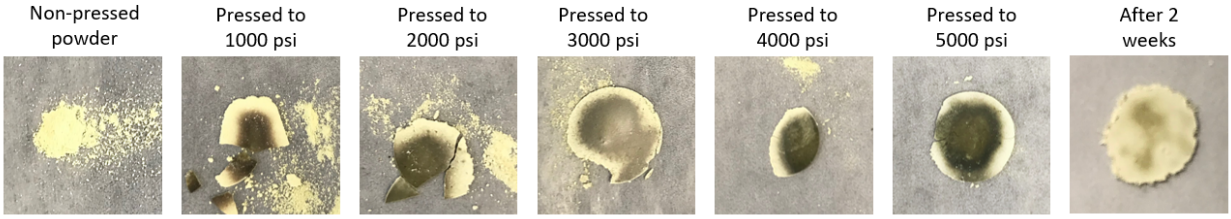

Figure 5. Photographs of the $Na_{0.20}WO_3 \cdot 0.81H_2O$ pellets prepared by pressing with increasing pressures. The photograph of the pellet pressed at 5000 psi after two weeks of storage is also shown.

An interesting color-change phenomenon was observed when pellets of the $Na_{0.20}WO_3 \cdot 0.81H_2O$ sample were pressed at 1000 psi and above (**Figure 5**). While the initial color of the synthesized material is a pale yellow, pressing at 1000 psi under a hydraulic press leads to a transition to a dark brown/black color. Upon pressure increase up to 5000 psi, the color becomes slightly darker and more uniform throughout the pellet. A pressure of 1000 psi corresponds to 70.3 kg cm^{-2} or 155.0 lbs. cm^{-2}, suggesting that if the entire weight of an average-sized human could be applied in a 1 cm^2 area (roughly the size of a thumb print), onto the surface of this $Na_{0.20}WO_3 \cdot 0.81H_2O$ sample, the described color change would be induced. This pressure effect is further intriguing due to its reversible nature. Pellets pressed at 5000 psi and then left in air for 2 weeks mostly returned to their original pale-yellow color. XRD patterns for pristine $Na_{0.20}WO_3 \cdot 0.81H_2O$ and this material pressed at 3000 psi can be seen in **Figure S3**. In addition, the pressed $WO_3 \cdot 1H_2O$ sample's XRD pattern (**Figure S3a**) reveals modification in relative intensities from preferred orientation and some peak broadening, possibly due to the sheets sliding one over another during the pressing, which could potentially cause nanoscale strains. Interestingly, no phase change is seen in the pressed $Na_{0.20}WO_3 \cdot 0.81H_2O$ sample (**Figure S3b**). Instead, a decrease in interplanar distances was observed upon pressing while the overall structure was maintained.

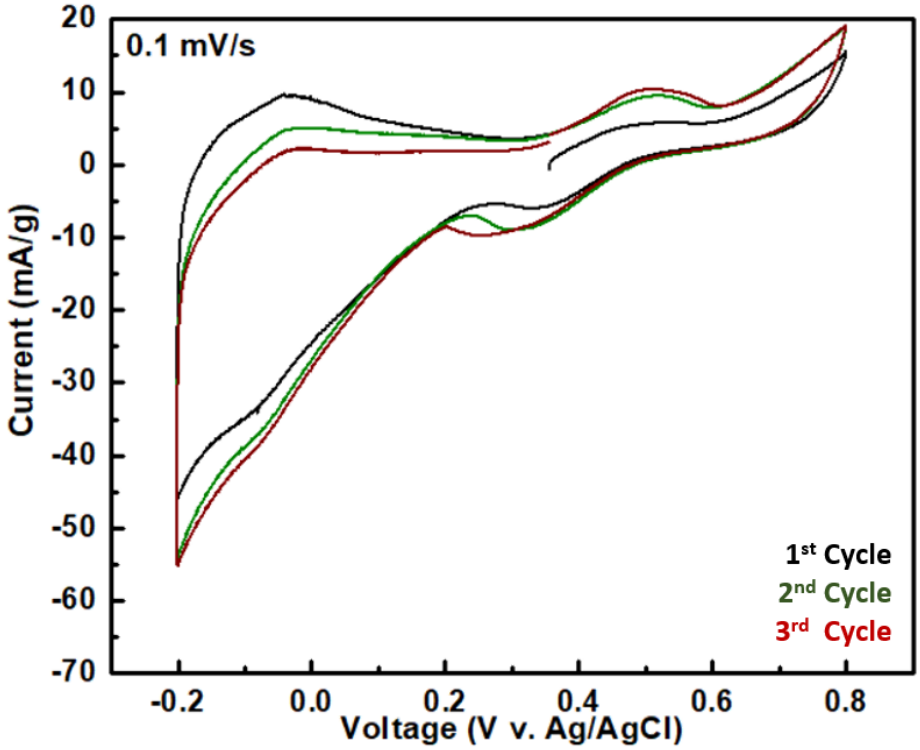

Figure 6. Cyclic voltammograms (CVs) of $Na_{0.20}WO_3 \cdot 0.81H_2O$ electrodes in aqueous cells with 1M H_2SO_4 electrolyte.

The results of electrochemical cycling of the $Na_{0.20}WO_3 \cdot 0.81H_2O$ electrode, allowing to evaluate the electrochemical activity of the new layered sodium tungstate in cells with aqueous and non-aqueous electrolytes are shown in **Figures 6, 7** and **S3**. Additional cycling in other aqueous-based electrolytes is shown in **Figure S4 (Supporting Information)**. In aqueous cells with $Na_{0.20}WO_3 \cdot 0.81H_2O$ electrode, aqueous acidic electrolyte and proton charge carriers, the shape of the CV curve has a shape with a rectangular area overlapping with broad reversible redox peaks (**Figure 6**). Such behavior resembles the pseudocapacitive proton storage that has been identified previously by Mitchell et al. for crystalline WO_3 and $WO_3 \cdot 2H_2O$ phases [8]. For $Na_{0.20}WO_3 \cdot 0.81H_2O$ cells, an initial discharge capacity of 37.43 mAh·g^{-1} (134.75 C·g^{-1}) was obtained due to the reduction of the W^{6+} ions within the structure. This initial capacity is on par with that achieved by crystalline WO_3 (136 C·g^{-1}), and significantly higher than that achieved by hydrated $WO_3 \cdot 2H_2O$ (45 C·g^{-1}), though it should be noted that these materials were cycled at a higher sweep rate of 1.0 mV s^{-1} [8]. The capacity of the $Na_{0.20}WO_3 \cdot 0.81H_2O$ electrode increases slightly over the first three cycles, with the highest capacity of 39.67 mAh·g^{-1} (142.81 C·g^{-1}) seen

on the third cycle, suggesting a slight activation of the electrode material. However, when cycled in cells with aqueous 1M NaOH or 1M Na_2SO_4 electrolytes, no electrochemical activity was demonstrated by the $Na_{0.20}WO_3 \cdot 0.81H_2O$ electrode **(Figure S4, Supporting Information**). This observation could be attributed to the nature of electrochemically cycled ions and the crystal structure of the chemically preintercalated $Na_{0.20}WO_3 \cdot 0.81H_2O$ phase. In fact, in basic and neutral electrolytes used in this work, large Na^+ ions are the charge carriers. The charge carrier intercalation into the structure of $Na_{0.20}WO_3 \cdot 0.81H_2O$ material could be inhibited by the presence of interlayer structural units in the interlayer region identified by the STEM imaging (**Figure 3b**). Therefore, further characterization of the charge storage behavior of the new Na-preintercalated tungsten oxide requires better understanding of the structure of this material.

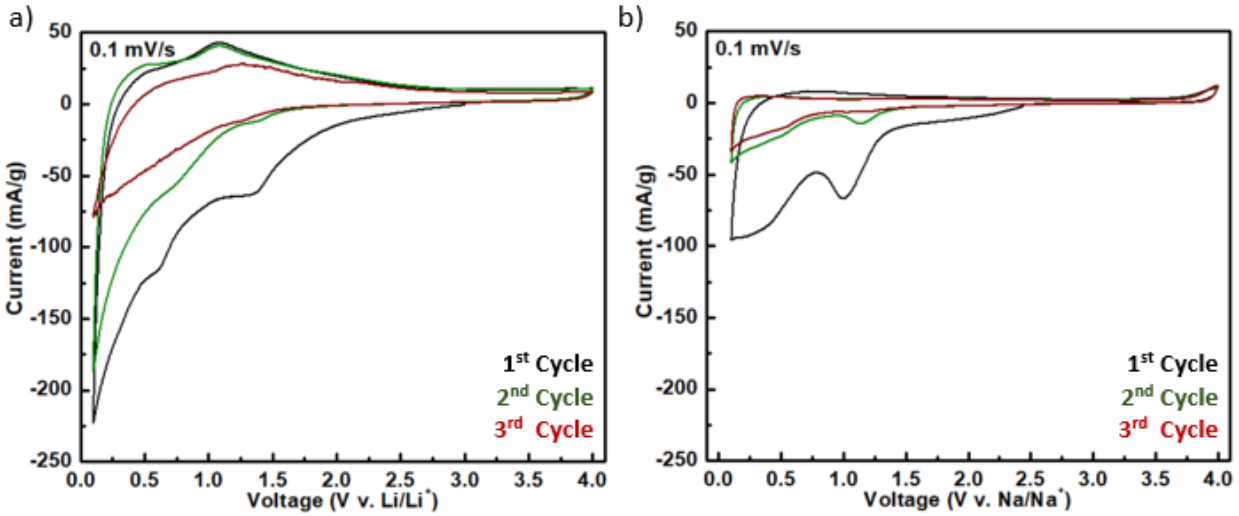

Figure 7. Cyclic voltammograms (CVs) of $Na_{0.20}WO_3 \cdot 0.81H_2O$ electrodes in non-aqueous (a) Li-ion and (b) Na-ion cells at a scan rate of 0.1 mV s^{-1}.

For non-aqueous systems, cells were cycled in a large voltage window from 0.1 – 4.0 V in order to identify any electrochemical activity of the phase (**Figure 7**). Like other tungsten oxide phases, the $Na_{0.20}WO_3 \cdot 0.81H_2O$ sample appears to be electrochemically active in the anodic region, with peaks detected below 2.0 V in both Li- and Na-ion cells [14-18]. In Li-ion cells, two peaks are found in the first discharge sweep in the CV curve which can be attributed to redox reactions (**Figure 7a**). The peak at ~1.5 V has not been observed previously for the pristine $WO_3 \cdot 1H_2O$ phase [14-16]. This peak likely corresponds to an irreversible redox process because a corresponding charge peak is not observed. The peak at ~0.6 V correlates well with peaks found

in CV curves for $WO_3 \cdot 1H_2O$ electrodes between 0.6 and 0.9 V during first discharge [14-16]. It should be noted, however, that this 0.6 V peak is of much lower intensity in our $Na_{0.20}WO_3 \cdot 0.81H_2O$ phase compared to those non-preintercalated materials. On the first discharge, the $Na_{0.20}WO_3 \cdot 0.81H_2O$ electrode showed an initial capacity of 480.8 $mAh \cdot g^{-1}$. This capacity drops to 257.2 $mAh \cdot g^{-1}$ in the second cycle where smaller peaks at 1.5 and 0.6V are observed. No peaks are visible in the third cycle for the $Na_{0.20}WO_3 \cdot 0.81H_2O$ phase that achieved a discharge capacity of 150.5 $mAh \cdot g^{-1}$. This significant first cycle irreversibility could be attributed to the destruction of the layered $Na_{0.20}WO_3 \cdot 0.81H_2O$ phase upon conversion, which has been determined to occur in other tungsten oxide phases [5, 14-16]. Further cycling could induce the nucleation of Li_2O, leading to lower overall capacities [5]. The 1.5 V peak observed only for the preintercalated $Na_{0.20}WO_3 \cdot 0.81H_2O$ phase suggests that the new layered structure found in this material leads to a change in its electrochemical behavior in Li-ion cells compared to the non-preintercalated $WO_3 \cdot 1H_2O$ material.

In Na-ion cells, two sharp peaks are visible in the first discharge sweep at 1.2 and 0.25 V, with a capacity of 253.2 mAh g^{-1} (**Figure 7b**). The CV curve of the $Na_{0.20}WO_3 \cdot 0.81H_2O$ phase in Na-ion cells looks decidedly different than any previously reported $WO_3 \cdot 1H_2O$ electrode [17, 18]. The significantly lower first discharge capacity in Na-ion cells compared to Li-ion cells may be due to the increased size of the charge carrier (i.e., Na^+ ions) in Na-ion cells. Na^+ ion diffusion may be hindered, similar to behavior seen in the basic and neutral aqueous electrolytes, due to the presence of bulky W^{6+} ions/WO_x polyhedra residing in the interlayer space. Further, both W^{6+} and Na^+ ions prefer octahedral sites, while Li^+ ions prefer tetrahedral sites. Therefore, it may be possible that a more limited number of octahedral sites are available for electrochemically cycled Na^+ ions. Cycling stability is also lower in Na-ion cells, with only 72 mAh g^{-1} obtained after the 2nd discharge cycle.

XRD patterns of the electrodes cycled in Li-ion and Na-ion cells after first discharge to 0.1 V are shown in **Figure S5** (**Supporting Information**). Based on the poor cyclability of the $Na_{0.20}WO_3 \cdot 0.81H_2O$ phase in Li-ion and Na-ion cells, as well as previous electrochemical studies on $WO_3 \cdot nH_2O$ phases, it was anticipated that the XRD patterns after first discharge would show peaks which correspond to M_2O (M=Li or Na). This product is the result of the tungsten oxide conversion reaction. Interestingly, no peaks for these products were seen. This result suggests two

possible conclusions: (1) these products are created after the conversion reaction, but due to the nano-structuring of the preintercalated nanoflakes and the low mass loading of the cycled electrodes (~0.5 mg cm^{-2}), the produced M_2O may not be detectable or (2) the conversion reaction seen in $WO_3 \cdot nH_2O$ electrochemical studies does not occur for this novel $Na_{0.20}WO_3 \cdot 0.81H_2O$ phase and the poor cyclability is due to other phenomena such as SEI formation. An improved understanding of the charge storage mechanism of the $Na_{0.20}WO_3 \cdot 0.81H_2O$ phase calls for a detailed electrochemical study which is outside of the scope of this work.

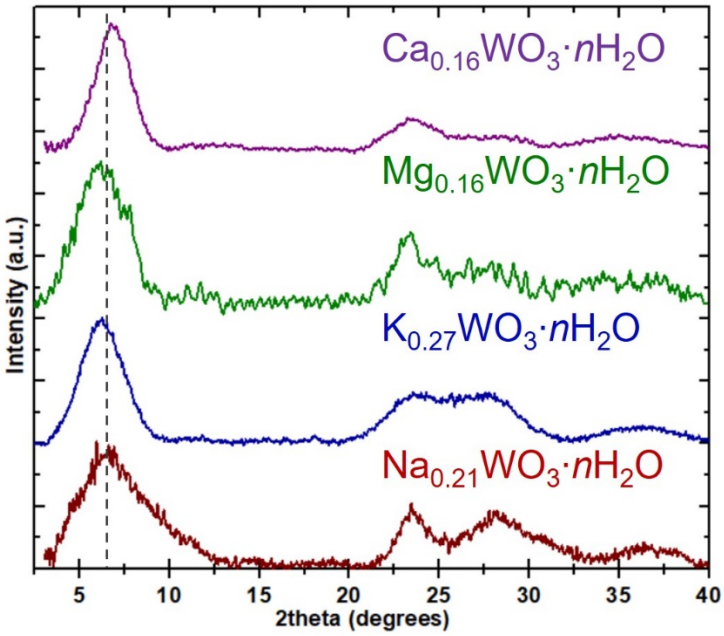

Figure 8. XRD patterns of the $M_xWO_3 \cdot nH_2O$ (M=Na, K, Mg, Ca) powders synthesized via chemical preintercalation synthesis approach. M:W ratio was evaluated using EDX spectroscopy. The dashed line is a reference to show slight differences in the positions of the peak of the highest intensity.

The chemical preintercalation synthesis of the never previously reported $Na_{0.20}WO_3 \cdot 0.81H_2O$ phase caused us to explore this strategy to prepare tungsten oxides with other cations. Following the same synthesis parameters, KCl, $MgCl_2$, or $CaCl_2$ was added to the reaction mixture with the aim to prepare preintercalated $M_xWO_3 \cdot nH_2O$ samples (M=K, Mg, and Ca). The XRD patterns of the produced materials are shown in **Figure 8**, with the XRD pattern of $Na_{0.20}WO_3 \cdot 0.81H_2O$ phase serving as a reference. XRD patterns show similar reflections implying that the synthesized

materials could be layered phases. The vertical dashed line shown between 5° and 10° 2θ is a reference to compare the positions of the highest intensity peak in the XRD patterns of the four synthesized phases. The peak maxima correspond to the slightly different 2θ values depending on the nature of the chloride salt used in the synthesis. However, this result is drastically different from the bilayered vanadium oxide family where the position of the highest intensity peak in the XRD patterns is highly dependent on the radius of the hydrated chemically preintercalated ion [21]. The M:W ratios for each sample, shown in **Figure 8**, were evaluated via EDX spectroscopy analysis. It should be noted that fewer Mg^{2+} and Ca^{2+} alkaline-earth ions are preintercalated as compared to the Na^{+} and K^{+} alkali ions. This may be due to the doubly charged nature of the Mg^{2+} and Ca^{2+} alkali earth ions compared to the singly charged alkali ions. Since the ions are co-intercalating together with water molecules during synthesis, larger hydrated alkaline-earth ions may require more space than smaller hydrated alkali ions which could lead to compositional diversity. These results demonstrate that the chemical preintercalation approach can be applied for the synthesis of open-layered transition metal oxides beyond vanadium and a versatile library of chemically preintercalated ions.

CONCLUSIONS

In this report, we have for the first time utilized the chemical preintercalation synthesis approach to prepare a new Na-containing, layered tungsten oxide phase, $Na_{0.20}WO_3 \cdot 0.81H_2O$. This structure is built from W-O layers with a d-spacing of 7.5 Å and W^{6+} ions or WO_x polyhedra residing in the interlayer region in periodic locations. The bonding behavior of this new Na-containing phase was shown to differ from the reference non-preintercalated compound $WO_3 \cdot nH_2O$. A reversible, pressure-induced color change from pale yellow to dark brown/black was observed for the $Na_{0.20}WO_3 \cdot 0.81H_2O$ sample when pressed at 1000 psi or higher. Initial cycling of the $Na_{0.20}WO_3 \cdot 0.81H_2O$ electrodes revealed that this material is electrochemically active in aqueous proton-based cells, non-aqueous Li-ion cells, and non-aqueous Na-ion cells. Application of the chemical preintercalation strategy to the synthesis of K-, Mg- and Ca-preintercalated tungsten oxides with similar structure introduces a new materials family for investigation.

AUTHOR INFORMATION

Corresponding Author

Tel: 215-571-4612 Fax: 215-895-6760

Email: ep423@drexel.edu

Author Contributions

E.P. developed the concept and designed the experiments. A.B. developed the altered chemical pre-intercalation synthesis method, carried out synthesis of all materials, ran XRD measurements, and performed aqueous-based electrochemical testing. M.C oversaw experiments, characterized material via SEM, EDS, Raman, and FTIR, and performed non-aqueous electrochemical testing. D.A.C. performed STEM imaging. All authors contributed to writing this manuscript.

ACKNOWLEDGEMENTS

We would like to thank the National Science Foundation (award numbers: DMR-1609272 and DMR-1752623) for funding. We acknowledge Drexel's Centralized Research Facilities as well as Bryan Byles from the Materials Electrochemistry Group at Drexel for assistance with materials characterization. STEM imaging was conducted at the Center for Nanophase Materials Sciences, which is a DOE Office of Science User Facility.

CONFLICT OF INTEREST STATEMENT

The authors declare that they have no known relationships or interests that could potentially influence or bias the submitted work.

REFERENCES

1. Costa, C., C. Pinheiro, I. Henriques, and C.A.T. Laia, *Inkjet Printing of Sol–Gel Synthesized Hydrated Tungsten Oxide Nanoparticles for Flexible Electrochromic Devices.* ACS Applied Materials & Interfaces, 2012. **4**(3): p. 1330-1340.
2. Deepa, M., A.G. Joshi, A.K. Srivastava, S.M. Shivaprasad, and S.A. Agnihotry, *Electrochromic Nanostructured Tungsten Oxide Films by Sol-gel: Structure and Intercalation Properties.* Journal of The Electrochemical Society, 2006. **153**(5): p. C365.
3. Gu, G., B. Zheng, W.Q. Han, S. Roth, and J. Liu, *Tungsten Oxide Nanowires on Tungsten Substrates.* Nano Letters, 2002. **2**(8): p. 849-851.
4. Alsawafta, M., Y.M. Golestani, T. Phonemac, S. Badilescu, V. Stancovski, and V.-V. Truong, *Electrochromic Properties of Sol-Gel Synthesized Macroporous Tungsten Oxide Films Doped with Gold Nanoparticles.* Journal of The Electrochemical Society, 2014. **161**(5): p. H276-H283.
5. Augustyn, V., *Tuning the interlayer of transition metal oxides for electrochemical energy storage.* Journal of Materials Research, 2017. **32**(1): p. 2-15.
6. Augustyn, V. and Y. Gogotsi, *2D Materials with Nanoconfined Fluids for Electrochemical Energy Storage.* Joule, 2017. **1**(3): p. 443-452.
7. Mitchell, J.B., N.R. Geise, A.R. Paterson, N.C. Osti, Y. Sun, S. Fleischmann, R. Zhang, L.A. Madsen, M.F. Toney, D.-e. Jiang, A.I. Kolesnikov, E. Mamontov, and V. Augustyn, *Confined Interlayer Water Promotes Structural Stability for High-Rate Electrochemical Proton Intercalation in Tungsten Oxide Hydrates.* ACS Energy Letters, 2019. **4**(12): p. 2805-2812.
8. Mitchell, J.B., W.C. Lo, A. Genc, J. LeBeau, and V. Augustyn, *Transition from Battery to Pseudocapacitor Behavior via Structural Water in Tungsten Oxide.* Chemistry of Materials, 2017. **29**(9): p. 3928-3937.
9. Wang, R., J.B. Mitchell, Q. Gao, W.-Y. Tsai, S. Boyd, M. Pharr, N. Balke, and V. Augustyn, *Operando Atomic Force Microscopy Reveals Mechanics of Structural Water Driven Battery-to-Pseudocapacitor Transition.* ACS Nano, 2018. **12**(6): p. 6032-6039.
10. Vidmar, T., M. Topj , P. Dzik, and U.O. Krbaovec, *Inkjet printing of soŒ gel derived tungsten oxide inks.* Solar Energy Materials and Solar Cells, 2014. **125**: p. 87-95.
11. Zheng, H., J.Z. Ou, M.S. Strano, R.B. Kaner, A. Mitchell, and K. Kalantar-zadeh, *Nanostructured Tungsten Oxide – Properties, Synthesis, and Applications.* Advanced Functional Materials, 2011. **21**(12): p. 2175-2196.
12. Wang, Z., W. Gong, X. Wang, Z. Chen, X. Chen, J. Chen, H. Sun, G. Song, S. Cong, F. Geng, and Z. Zhao, *Remarkable Near-Infrared Electrochromism in Tungsten Oxide Driven by Interlayer Water-Induced Battery-to-Pseudocapacitor Transition.* ACS Applied Materials & Interfaces, 2020. **12**(30): p. 33917-33925.
13. Kim, E., S. Suzuki, and M. Miyayama, *Electrode properties of layered tungsten-based oxides for electrochemical capacitors.* Journal of the Ceramic Society of Japan, 2014. **122**(1426): p. 426-429.
14. Yoon, S., C. Jo, S.Y. Noh, C.W. Lee, J.H. Song, and J. Lee, *Development of a high-performance anode for lithium ion batteries using novel ordered mesoporous tungsten oxide materials with high electrical conductivity.* Physical Chemistry Chemical Physics, 2011. **13**(23): p. 11060-11066.
15. Li, W.-J. and Z.-W. Fu, *Nanostructured WO3 thin film as a new anode material for lithium-ion batteries.* Applied Surface Science, 2010. **256**(8): p. 2447-2452.
16. Kim, D.-M., S.-J. Kim, Y.-W. Lee, D.-H. Kwak, H.-C. Park, M.-C. Kim, B.-M. Hwang, S. Lee, J.-H. Choi, S. Hong, and K.-W. Park, *Two-dimensional nanocomposites based on tungsten oxide nanoplates and graphene nanosheets for high-performance lithium ion batteries.* Electrochimica Acta, 2015. **163**: p. 132-139.
17. Ryu, W.-H., H. Wilson, S. Sohn, J. Li, X. Tong, E. Shaulsky, J. Schroers, M. Elimelech, and A.D. Taylor, *Heterogeneous WSx/WO3 Thorn-Bush Nanofiber Electrodes for Sodium-Ion Batteries.* ACS Nano, 2016. **10**(3): p. 3257-3266.

18. Santhosha, A.L., S.K. Das, and A.J. Bhattacharyya, *Tungsten Trioxide (WO3) Nanoparticles as a New Anode Material for Sodium-Ion Batteries.* Journal of Nanoscience and Nanotechnology, 2016. **16**(4): p. 4131-4135.
19. Clites, M., B.W. Byles, and E. Pomerantseva, *Effect of aging and hydrothermal treatment on electrochemical performance of chemically pre-intercalated Na–V–O nanowires for Na-ion batteries.* Journal of Materials Chemistry A, 2016. **4**(20): p. 7754-7761.
20. Clites, M., J.L. Hart, M.L. Taheri, and E. Pomerantseva, *Chemically Preintercalated Bilayered KxV2O5·nH2O Nanobelts as a High-Performing Cathode Material for K-Ion Batteries.* ACS Energy Letters, 2018. **3**(3): p. 562-567.
21. Clites, M. and E. Pomerantseva, *Bilayered vanadium oxides by chemical pre-intercalation of alkali and alkali-earth ions as battery electrodes.* Energy Storage Materials, 2018. **11**: p. 30-37.
22. Dong, Y., X. Xu, S. Li, C. Han, K. Zhao, L. Zhang, C. Niu, Z. Huang, and L. Mai, *Inhibiting effect of Na+ pre-intercalation in MoO3 nanobelts with enhanced electrochemical performance.* Nano Energy, 2015. **15**: p. 145-152.
23. Yao, X., Y. Zhao, F.A. Castro, and L. Mai, *Rational Design of Preintercalated Electrodes for Rechargeable Batteries.* ACS Energy Letters, 2019. **4**(3): p. 771-778.
24. Mai, L.Q., B. Hu, W. Chen, Y.Y. Qi, C.S. Lao, R.S. Yang, Y. Dai, and Z.L. Wang, *Lithiated MoO3 Nanobelts with Greatly Improved Performance for Lithium Batteries.* Advanced Materials, 2007. **19**(21): p. 3712-3716.
25. Clites, M., R. Andris, D.A. Cullen, K.L. More, and E. Pomerantseva, *Improving Electronic Conductivity of Layered Oxides through the Formation of Two-Dimensional Heterointerface for Intercalation Batteries.* ACS Applied Energy Materials, 2020. **3**(4): p. 3835-3844.
26. Clites, M. and E. Pomerantseva, *Synthesis of hybrid layered electrode materials via chemical pre-intercalation of linear organic molecules*. SPIE Nanoscience + Engineering. Vol. 10725. 2018: SPIE.
27. Wei, Q., Z. Jiang, S. Tan, Q. Li, L. Huang, M. Yan, L. Zhou, Q. An, and L. Mai, *Lattice Breathing Inhibited Layered Vanadium Oxide Ultrathin Nanobelts for Enhanced Sodium Storage.* ACS Applied Materials & Interfaces, 2015. **7**(33): p. 18211-18217.
28. Mukherjee, S., C.D. Quilty, S. Yao, C.A. Stackhouse, L. Wang, K.J. Takeuchi, E.S. Takeuchi, F. Wang, A.C. Marschilok, and E. Pomerantseva, *The effect of chemically preintercalated alkali ions on the structure of layered titanates and their electrochemistry in aqueous energy storage systems.* Journal of Materials Chemistry A, 2020. **8**(35): p. 18220-18231.
29. Supothina, S., P. Seeharaj, S. Yoriya, and M. Sriyudthsak, *Synthesis of tungsten oxide nanoparticles by acid precipitation method.* Ceramics International, 2007. **33**(6): p. 931-936.
30. Ingham, B., S.V. Chong, and J.L. Tallon, *Layered tungsten oxide-based hybrid materials incorporating transition metal ions.* Current Applied Physics, 2006. **6**(3): p. 553-556.
31. Park, C.Y., J.M. Seo, H. Jo, J. Park, K.M. Ok, and T.J. Park, *Hexagonal tungsten oxide nanoflowers as enzymatic mimetics and electrocatalysts.* Scientific Reports, 2017. **7**(1): p. 40928.
32. Moretti, A., G. Giuli, A. Trapananti, and S. Passerini, *Electrochemical and structural investigation of transition metal doped V2O5 sono-aerogel cathodes for lithium metal batteries.* Solid State Ionics, 2018. **319**: p. 46-52.
33. Petkov, V., P.N. Trikalitis, E.S. Bozin, S.J.L. Billinge, T. Vogt, and M.G. Kanatzidis, *Structure of V2O5·nH2O Xerogel Solved by the Atomic Pair Distribution Function Technique.* Journal of the American Chemical Society, 2002. **124**(34): p. 10157-10162.
34. Daniel, M.F., B. Desbat, J.C. Lassegues, B. Gerand, and M. Figlarz, *Infrared and Raman study of WO3 tungsten trioxides and WO3, xH2O tungsten trioxide tydrates.* Journal of Solid State Chemistry, 1987. **67**(2): p. 235-247.
35. Pang, H.-F., X. Xiang, Z.-J. Li, Y.-Q. Fu, and X.-T. Zu, *Hydrothermal synthesis and optical properties of hexagonal tungsten oxide nanocrystals assisted by ammonium tartrate.* physica status solidi (a), 2012. **209**(3): p. 537-544.

36. Kalantar-zadeh, K., A. Vijayaraghavan, M.-H. Ham, H. Zheng, M. Breedon, and M.S. Strano, *Synthesis of Atomically Thin WO3 Sheets from Hydrated Tungsten Trioxide.* Chemistry of Materials, 2010. **22**(19): p. 5660-5666.
37. Xu, L., M.-L. Yin, and S. Liu, *Agx@WO3 core-shell nanostructure for LSP enhanced chemical sensors.* Scientific Reports, 2014. **4**(1): p. 6745.